Current-Induced Nucleation and Motion of Skyrmions in Zero Magnetic Field

Sougata Mallick, Sujit Panigrahy, Gajanan Pradhan, Stanislas Rohart

Current-Induced Nucleation and Motion of Skyrmions in Zero Magnetic Field

Sougata Mallick,* Sujit Panigrahy, Gajanan Pradhan, and Stanislas Rohart†
Laboratoire de Physique des Solides, Université Paris-Saclay, CNRS UMR 8502, Orsay Cedex F-91405, France

(Received 4 April 2022; revised 30 September 2022; accepted 23 November 2022; published 23 December 2022)

We study the stabilization and electrical manipulation of skyrmions in magnetic ultrathin films in the absence of an applied magnetic field. We show that this requires an increased magnetic anisotropy, controlled by the sample thickness, as compared to usual skyrmionic samples, so that the uniform state corresponds to the zero-field ground state and the skyrmions to metastable excitations. Although skyrmion stabilization at zero field is demonstrated over a broad range of thicknesses, electrical control appears to be more demanding to avoid skyrmion deformation. In the thinnest samples, the large magnetic anisotropy prevents skyrmion deformations and we show that they can be nucleated progressively by current pulses, which underlines that the only possible transition occurs between uniform and skyrmion states. The solitonic skyrmions in zero applied magnetic field have the same properties as compared to field-stabilized ones, with a long-term stability and high mobility when excited by a spin-orbit torque.

DOI: 10.1103/PhysRevApplied.18.064072

I. INTRODUCTION

Magnetic skyrmions are appealing magnetic textures to develop innovating spintronic devices and applications [1–3]. In that perspective, the information process is based on the controlled nucleation and motion of individual skyrmions that are considered as solitons [4,5]. Therefore, the magnetic materials should not host arrays of skyrmions but metastable excitations over a homogeneous magnetization ground state [6]. To this aim, in most studies [5,7–12], the application of a magnetic field is required in order to promote a uniform ground state over which metastable skyrmions can be manipulated individually. However, as illustrated by several theoretical works, solitonic skyrmions can exist even in zero applied field [4,13,14]. From the application point of view, avoiding an applied magnetic field sounds appealing to reduce the complexity and enhance the device efficiency. In the perspectives of using antiferromagnetic materials (real antiferromagnets [15], as well as ferrimagnets [16,17] or synthetic antiferromagnets [18,19]), where samples are not sensitive to an external field, the ability to stabilize skyrmions at remanence is crucial.

The possibility of stabilizing skyrmions in the absence of an external field has received great attention and has led to different successful routes. An elegant possibility is the substitution of the external magnetic field by a built-in internal field, induced, for example, by exchange bias at the interface with an antiferromagnetic layer [20,21] or by an Ruderman-Kittel-Kasuya-Yoshida (RKKY) induced coupling from a homogeneous ferromagnetic layer through a well-chosen nonmagnetic spacer [19]. Some samples also enable researchers to get rid of any bias field, through either geometrical confinement [9,22,23], a particular magnetic field history [24,25], micromagnetic parameter optimization [17,26,27], or via thermal effects [28] or strong frustration of the exchange interaction [29]. However, the solitonic character of the observed skyrmions is yet to be demonstrated. Indeed, beyond the observation of nontrivial topological and compact domains, the control and nucleation by current of nondeformable textures would provide a real proof of the skyrmionic character, so that zero-field skyrmions could open up significant perspectives in the field of skyrmion-based devices.

In this paper, we study the dynamics of zero-field magnetic skyrmions in a Pt/Co/Au-based multilayer. Close to the magnetic anisotropy compensation, samples display a spontaneous stripe demagnetization pattern at zero field, as observed in most skyrmion host materials [5,7–12]. When reducing the Co-layer thickness, the increase of the magnetic anisotropy improves the uniform state stability and there is a thickness range in which uniform, stripe, and skyrmionlike states are stable at zero field, depending on the sample magnetic history. We study the dynamics of these excitations in connected patterned samples. The observation of zero-field skyrmionlike textures, obtained from a field process, is found to be an insufficient condition to enable their current-induced control. In particular, the ability to nucleate skyrmions directly from the uniformly magnetized state is indeed a challenging process, since no specific final state is promoted, contrary to the experiments at finite magnetic field [10,12,30]. The variety

*sougata.physics@gmail.com
†stanislas.rohart@universite-paris-saclay.fr

of possible excited states implies that a high optimization of the sample parameters is required, so that the skyrmion is the only outcome of a current-induced nucleation experiment. In the best samples, we show that the textures are true zero-field skyrmions: they can be nucleated from the uniform magnetic state using standard current-nucleation techniques [10,12,30] and they obey behavior similar to that of field-stabilized skyrmions [5,12,31,32], including gyrotropic deflection and velocities greater than 70 m/s.

II. EXPERIMENTAL DETAILS

Our samples are based on a Co magnetic bilayer with symmetric stacking, following the approach of Hrabec *et al.* [12,33]. They are grown on a Si(100) highly resistive substrate, oxydized over 100 nm and covered by a 3-nm Ta seed layer. The stack of interest is Pt(5)/Co(t_{Co})/Au(2.5)/Co(t_{Co})/Pt(5) (all thicknesses are given in nanometers; see the Supplemental Material [34]). In such a heterostructure, magnetic textures (domain walls or skyrmions, depending on the magnetic parameters) with opposite chirality in each layer are coupled by dipolar interaction and are sensitive to spin-orbit torques induced by the charge-to-spin conversion in both Pt outer layers. The Pt-Co interface provides a large Dzyaloshinskii-Moriya interaction (DMI) [35] with $D_s = 0.66 \pm 0.1$ pJ/m [33,36]. The Pt-layer thickness enables efficient charge-to-spin conversion and therefore a large spin-orbit torque gets induced to the Co layers. The Au thickness is sufficient to avoid any exchange coupling between the Co layers [33,37], which are only coupled through dipolar interaction. In this symmetric stack, the chirality is not only given by the DMI but also by the flux closure at the domain walls or transition regions [12,38], which increase the total chiral energy [33]. The Co thicknesses are tuned between 1.30 and 1.60 nm in order to modify the magnetic anisotropy. As measured on samples with a single Co layer, the interface (K_S/t_{Co}) and shape ($-\frac{1}{2}\mu_0 M_S^2$) magnetic anisotropies compensate each other at approximately 1.65–1.70 nm, where the effective magnetic anisotropy [39] $K_{\mathrm{eff}} = K_S/t_{\mathrm{Co}} - \frac{1}{2}\mu_0 M_S^2$ is close to zero. Using $M_S = 1.55 \times 10^6$ A/m^2, the interfacial anisotropy energy is therefore estimated to be $K_S = 2.55 \pm 0.10$ mJ/m^2 (see the Supplemental Material [34]). The Co thickness is varied in steps of 0.5 Å. While such a step is below the atomic layer thickness, the magnetic layer roughness is not impacted, since the layers are not epitaxial and consist of grains of (10–15)-nm diameter. Similarly, the texture-pinning landscape (relevant for the skyrmion motion, as well as for the texture-morphology evolution) is not affected by the roughness eventually induced by partial atomic layers, since it is mostly related to the granular structure, as demonstrated in earlier studies [40]. Current-induced nucleation and motion has been studied in (1–3)-μm tracks obtained using electron-beam lithography and Ar^+ etching, connected by Ti-Au contacts. Magnetic textures have been observed using magnetic force microscopy (MFM) using home-built soft-MFM tips with a (Co-Cr)/Cr–bilayer coating to reduce tip-induced perturbation of magnetic textures (see Refs. [12,41,42] and the Supplemental Material [34]).

III. SKYRMION STABILIZATION AT ZERO APPLIED FIELD

Magnetic textures arise from the equilibrium between all the micromagnetic energies. To describe skyrmions, the two key parameters are the domain-wall energy $\sigma = 4\sqrt{AK_{\mathrm{eff}}} - \pi D$ [13] (A is the exchange-energy constant) and the long-range dipolar coupling [6,9,43,44]. A large DMI lowers the domain-wall energy and can destabilize the uniform state for $D > 4\sqrt{AK_{\mathrm{eff}}}/\pi$ [13]. Long-range dipolar couplings promote a demagnetized state by creating a flux-closure situation between up- and down-magnetization regions and provide another mechanism to create magnetic textures. However, such an effect is limited in ultrathin films, and below a film thickness of $\sigma/\mu_0 M_S^2$, their influence is not significant [9,43]. These two criteria provide guidelines for material optimization through the magnetic film thickness, so that the relative energy of uniform and noncollinear magnetization phases can be tuned.

Close to the magnetic anisotropy compensation thickness, where $K_{\mathrm{eff}} \approx 0$, the samples spontaneously demagnetize, as shown in Fig. 1(a), for a $t_{\mathrm{Co}} = 1.60$ nm thick sample, since both criteria defined above are satisfied [9,12]. In such samples, the remanent state always corresponds to a disordered stripe phase (see Fig. S3 in the Supplemental Material [34]), whatever the magnetic history, as underlined by the minor loops in Fig. 1(a). This result is a direct consequence of the low effective magnetic anisotropy and therefore low domain-wall energy. Under the action of the DMI and/or the dipolar couplings, the creation of stable domains with a reversed magnetization is energetically favorable. Textures can proliferate; hence the destabilization of the uniform magnetization state. Upon the application of a perpendicular magnetic field close to the saturation, isolated (85–150)-nm-diameter skyrmions are observed [Fig.1(b)], with a core oriented antiparallel to the applied field. However, when releasing the external field, these skyrmions turn out to be unstable. As shown in Fig. 1(c), they spontaneously expend to form wormlike domains, in order to maximize the length of the domain walls, an effect similar to the run-out instability introduced to describe magnetic bubbles [45]. Note that this remanent state is slightly different from the true demagnetized state, which is attributed to a small energy barrier to nucleate additional stripes.

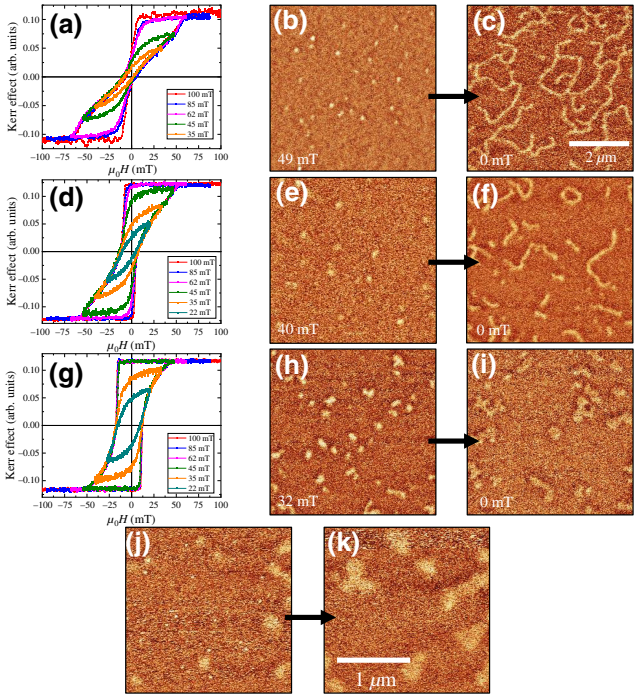

FIG. 1. The (a),(d),(g) hysteresis loops, (b),(e),(h),(j) field-stabilized skyrmion states, and the following relaxed state in (c),(f),(i),(k) zero-field MFM images, for different Co thicknesses [(a)–(c) $t_{Co} = 1.6$ nm, (d)–(f) $t_{Co} = 1.55$ nm, (g)–(i) $t_{Co} = 1.5$ nm]. The hysteresis loops are taken for different maximum fields as shown in the legends, to display full and minor loops. The field-stabilized skyrmion images are taken close to the magnetic saturation, at approximately (b) 49, (e) 40, and (h) 32 mT, respectively. They display skyrmions with approximately (b) (85–150)-nm, (e) (110–170)-nm, and (h) (150–300)-nm diameters, respectively. All images have the same size, indicated in (c). Images (j) and (k) correspond to a closer view of the $t_{Co} = 1.5$ nm sample, both taken at exactly the sample location, and show how the textures relax at zero magnetic field, from a field-stabilized state.

Decreasing the Co thickness increases the effective magnetic anisotropy. From 1.55 nm and below, the hysteresis loops have an approximately 100% remanent magnetization, showing that the stability of the uniform state is improved. Below 1.20 nm, square loops are observed, which indicates that the magnetic anisotropy is so large that up or down uniform states are the only stable states [33]. However, the transition from zero remanent to square loops is continuous, with a rich variety of loops observed between 1.30 and 1.55 nm (see the Supplemental Material [34]). In this thickness range, despite the 100% remanence, the magnetic state does not switch abruptly to the reversed uniform state but to intermediate states that contain magnetic textures, as shown in Figs. 1(e) and 1(h) for $t_{Co} = 1.55$ and 1.50 nm. This is interpreted as a thickness range with an intermediate domain-wall energy, sufficiently large to avoid self-demagnetization at zero field but that still enables magnetic textures. This is also underlined by the fact that these samples can easily be demagnetized through a conventional demagnetization protocol and minor loops as shown in Figs. 1(d) and 1(g). Close to the magnetic saturation, isolated skyrmions are stabilized for Co thicknesses of 1.50 and 1.55 nm. In these states, the skyrmion core is antiparallel to the applied magnetic field, which maintains a small and compact shape.

From the field-stabilized skyrmion state, releasing the applied magnetic field shows different behavior. In the 1.55-nm-thick sample, the domain-wall energy is still too low to prevent a run-out instability, which results in a zero-field magnetic state similar to that in thicker samples, although with a more limited domain expansion. On the contrary, for $t_{Co} = 1.5$ nm [see Figs. 1(g)–1(i)], the larger anisotropy and domain-wall energy prevent the instability and the skyrmions remain rather compact in zero field. The main evolution is a diameter increase, since the applied field is compressing to the skyrmion core. However, small deformations (moderate anisotropic expansion, flowerlike shapes $\cdots$) cannot be avoided, which shows that the texture morphology is close to being unstable. Even if they probably keep to skyrmion topology, like any domains in chiral magnetic samples, they are certainly too fragile to be used as zero-field skyrmions. Note, however, that the long-term stability of these states at zero field is good, as checked by imaging the same sample after several hours without any noticeable change (see the Supplemental Material [34]).

It is tempting to further decrease the Co thicknesses to improve the shape stability at zero magnetic field. Indeed, the larger magnetic anisotropy should induce a larger domain-wall energy and should suppress the run-out instability, following the trend observed from 1.60-nm to 1.50-nm Co thickness. Between 1.30-nm and 1.45-nm Co thickness, the hysteresis loops are not perfectly square and show that some intermediate textured states are possible. However, only stripes or wormlike states can be observed during the field process, with an abrupt transition from stripes to the homogeneous state when increasing the field (see the Figs. S2 and S4 in the Supplemental Material [34]). In these samples, the stabilization of skyrmions using a field-sweeping procedure looks impossible.

Samples with a 100% remanence enable the stabilization of different magnetic states at zero field (density and morphology changes), depending on the magnetic history, as visible in the minor loops in Figs. 1(d) and 1(g). Contrary to a sample where the homogeneous state is not stable in zero field, here, the textures stabilized at a given applied field remain relatively stable at zero field, without any parasitic nucleation of new textures. This is illustrated in the $t_{Co} = 1.50$-nm sample, shown in Fig. 2. Using a standard demagnetization process (sinusoidal field sweeping, with a progressive amplitude reduction), a disordered stripe phase, similar to that observed in a self-demagnetizing

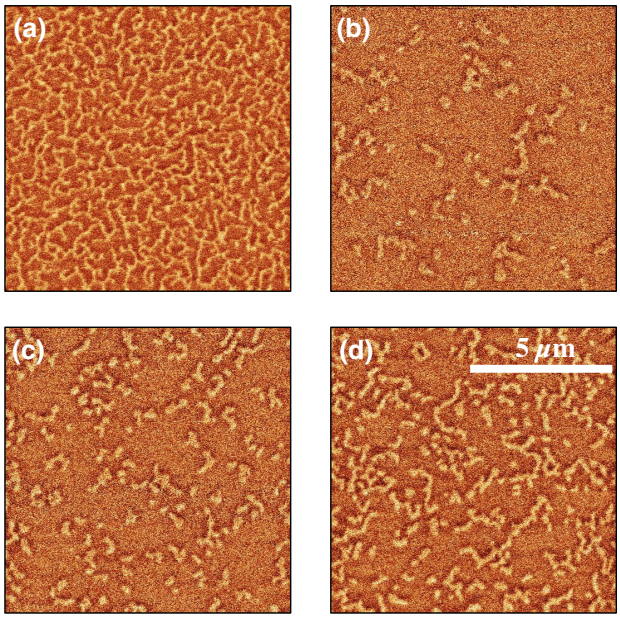

FIG. 2. (a)–(d) MFM images captured at magnetic remanence in the bilayer sample with $t_{Co} = 1.50$ nm: (a) after a standard demagnetization procedure; and (b)–(d) at zero field, following a saturation in negative field and the application of 32, 28, and 24 mT, respectively.

sample, is obtained [Fig. 2(a)]. After the application of a field smaller than the saturation field, different states are stabilized at remanence. They correspond to a continuous evolution (isotropic and anisotropy expansion) of the textures stabilized at the applied field. Note that the larger the last applied field is, the more compact are the textures at remanence.

IV. ZERO-FIELD SKYRMION CURRENT CONTROL

In Sec. III, skyrmionlike magnetic textures are stabilized at zero applied magnetic field from an existing skyrmion state close to the saturation field. Provided that no run-out instability occurs at zero field, this process is straightforward, involving a continuous evolution from the field-stabilized texture, without any modification of the topology. On the contrary, skyrmion nucleation directly from the uniformly magnetized state is a more challenging process. Indeed, a topology change is required and no specific final state is promoted. When a field is applied close to the magnetic saturation, textures that contain magnetic moments oriented antiparallel to the applied field are so unfavored that skyrmions are generally the most likely excited state, as demonstrated in several experiments [10,12,30]. At zero applied magnetic field, the variety of possible magnetic states, as underlined by the observations in Fig. 2, leads to more complexity and uncertainty. It is therefore highly demanding on the material optimization, so that skyrmions become the most favorable nucleated result. Beyond an obvious applied interest, such a nucleation experiment provides a test of the different accessible states and their relative energy.

These problematics are investigated using current-induced nucleation in the vicinity of sharp electrodes in magnetic tracks (see the Supplemental Material [34]), using a protocol previously developed for nucleation at finite fields [12]. We consider devices with 1-μm- or 3-μm-wide tracks, connected by Ti-Au contacts. On one side, the contact consists of a sharp electrode, whereas on the other the contact is flat across the wire and does not provide any current concentration. At the sharp-contact, current concentration, current line divergence, heating, and spin accumulation may occur and participate in the nucleation [28,46–48]. However, considering the symmetry of the multilayer stack and the current-injection geometry, the Oersted field associated with the current is negligible close to the contact, where skyrmions are created [12] and should play a limited role. Before each set of measurements, the device is saturated using a perpendicular magnetic field and short (2–7)-ns-long current pulses are applied in the absence of any external field.

Even if zero-field skyrmionlike texture stabilization is possible for $t_{Co} = 1.50$ nm from a field procedure, the application of a current pulse leads to a demagnetization of the whole track and the formation of a stripe phase. Indeed, in these samples, the nucleation energy barrier is so small that the global track heating easily destabilizes the uniform state, a result similar to the work of Lemesh *et al.* [28]. Improved results could be obtained with thinner samples. For samples with $t_{Co} = 1.35$ nm, the application of current pulses ($J = 0.4 \times 10^{12}$ A/m^2, 5 ns) leads to the formation of stripes only in the vicinity of the sharp contact. This indicates that the nucleation energy barrier is increased as compared to the previous samples and that textures can be nucleated only in the hottest part of the sample. In this sample, skyrmions are not obtained, since the stripe phase is likely to have a lower energy, but this result still indicates an increase in texture energy. This is coherent with the approach developed in Sec. III, where the domain-wall energy is increased by decreasing the Co thickness. The application of current pulses to the $t_{Co} = 1.30$ nm sample leads to the nucleation of compact skyrmionic textures in the vicinity of the sharp contact. In this sample, the larger domain-wall energy prohibits the elongation of the texture after the formation of a small nucleus and the compact shape is retained. Note that this result is obtained in a sample where the thickness is so small that the hysteresis loop is almost square (see the Supplemental Material [34]), indicating that any texture has an energy significantly larger than that of the homogeneous state. The difference between the $t_{Co} = 1.30$ nm sample and the thicker samples underlines that, here, the skyrmion state is well separated in

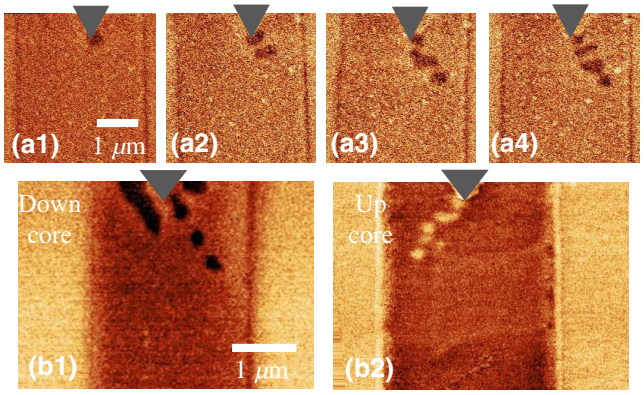

FIG. 3. (a1)–(a4) The current-induced nucleation in the vicinity of a sharp contact (triangular notch at the top of each image) on the $t_{Co} = 1.30$-nm-bilayer samples, in a 3-μm-wide track. Starting from a saturated state (not shown), a single current pulse ($J = 0.85 \times 10^{12}$ A/m^2 for 4 ns) is applied between two successive images. (b1),(b2) The nucleation of skyrmions followed by the application of three [(b1), down core)] and four [(b2), up core)] current pulses ($J = 0.85 \times 10^{12}$ A/m^2 for 5 ns), respectively.

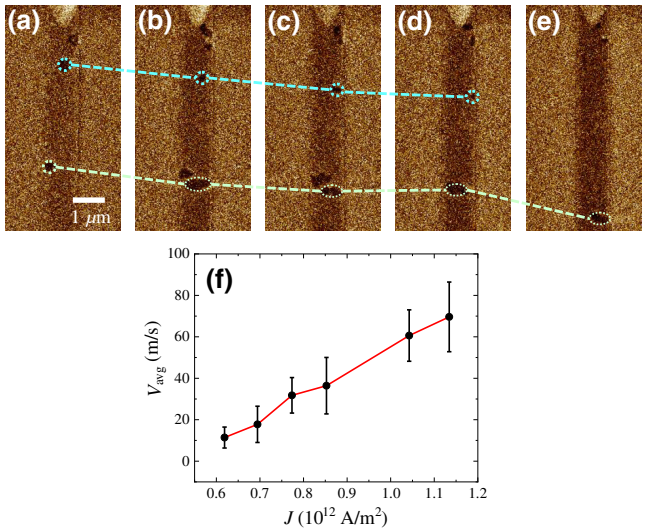

FIG. 4. (a)–(e) The motion of skyrmions under the influence of a series of current pulses ($J = 1.13 \times 10^{12}$ A/m^2 for 4 ns) for the sample with $t_{Co} = 1.30$ nm. The dashed circles and lines represent the positions and movements of the skyrmions, respectively. (f) The velocity (v_{avg}) versus the current density (J) plot for sample with $t_{Co} = 1.30$ nm. The error bar in (f) corresponds to the difference of the velocities between the fastest and slowest skyrmions in between two successive electrical pulses.

energy from the other texture, making their nucleation the most likely result, independent of the precise nucleation mechanism.

Figures 3(a1)–(a4) show the skyrmion nucleation experiments in the $t_{Co} = 1.30$ nm sample, using a 3-μm-wide track. A single current pulse of $J = 0.85 \times 10^{12}$ A/m^2 for a duration of 4 ns is applied between two successive images, starting from a uniform state (all spins saturated toward the up orientation—not shown here). The current flows from the sharp electrode (represented by the gray triangle on the top of each image) toward the flat electrode. Compact magnetic textures appear in the vicinity of the electrode with a core polarity (dark) opposite to the initial saturation direction, as expected for any excited texture over a uniform magnetic state. The dark contrast corresponds to an attractive force and hence a skyrmion core parallel to the microscope tip magnetization. Figures 3(a1)–(a4) show a succession of images to demonstrate that the process is progressive. In this experiment, each pulse nucleates exactly one skyrmion and pushes the existing ones, forming a train of almost equally spaced skyrmions. Further, Figs. 3(b1) and 3(b2) show the nucleation of skyrmions followed by application of three current pulses ($J = 0.85 \times 10^{12}$ A/m^2 for 5 ns) but starting from initial uniform states with opposite magnetic orientation. The skyrmions that are nucleated hence have opposite core polarization, as indicated by the opposite contrast in the MFM images. This demonstrates that the process of nucleation is independent of the core polarization. The nucleated skyrmions are deflected toward the right or the left, respectively, depending on the skyrmion-core polarization. This behavior is a direct consequence of the topological character of the skyrmions. Due to their particular topology, skyrmions traveling at a velocity $\mathbf{v}$ undergo a gyrotropic force $\mathbf{G} \times \mathbf{v}$, with $\mathbf{G} = (M_S t_{Co}/\gamma) S\mathbf{z}$ (γ is the gyromagnetic ratio), which induces a deflection, the direction of which depends on the topological number S. Since an opposite skyrmion core leads to an opposite topological number [49], this force explains the opposite deflection direction.

The skyrmion-current-induced motion in the $t_{Co} = 1.30$-nm-thick sample is further studied in 1-μm-wide tracks where the skyrmions are better confined. Current pulses with varying intensity J and duration from 4 to 10 ns are used to move the skyrmions at zero applied field. Figures 4(a)–4(e) show the motion of skyrmions under the influence of a series of current pulses ($J = 1.13 \times 10^{12}$ A/m^2 for 4 ns). The dashed circles and lines represents the positions and movements of the skyrmions, respectively. The direction of the current pulse is from the point contact toward the flat electrode (top to down) in the sample. The skyrmions are pushed along the current direction, which suggests that the motion is induced by the spin Hall effect in the Pt layers, as expected, considering that the Pt-Co interface DMI induces a left-handed chirality [12,35,50,51]. It can be observed that the movement of the skyrmions in between two pulses is not uniform and eventually differs from one skyrmion to the other. This is associated with the role of defects and skyrmion motion mostly occurs by

hopping within the inhomogeneous pinning landscape of the sample, which limits their velocity [52]. Further, the skyrmions either annihilate or remain pinned once they reach the side of the magnetic tracks. Figure 4(f) shows the average velocity v_{avg} versus the current density. A pinning threshold of about 0.5×10^{12} A/m^2 is observed, a bit higher than the best published results, probably due to the high pinning at the Co-Au interface [53]. However, the skyrmion mobility is comparable to the best results with a maximum average velocity of approximately 70 m/s, obtained at 1.13×10^{12} A/m^2. The application of current pulses with a larger J leads to skyrmion deformations or further nucleation within the track. At the largest current densities, a stripe phase is formed in the whole track. The skyrmion motion under a few other current densities and pulses is presented in the Supplemental Material [34].

V. CONCLUSIONS

In this work, we show that magnetic skyrmions can be stable in the absence of an external magnetic field if the sample micromagnetic parameters are finely tuned via the sample thickness. Contrary to the usual approaches that enable field-stabilized skyrmions, this requires samples with a finite perpendicular magnetic anisotropy, to prevent the skyrmions from being converted to elongated structures (run-out instability). The ability to stabilize skyrmionlike textures from the field process is found to be an insufficient condition to enable their use in skyrmion-based spintronic devices. Indeed, when excited by current, some skyrmions can be deformed into elongated structures. Robust skyrmions the shape of which remains compact during the motion require an even larger anisotropy and therefore an accurate optimization process. In these conditions, the skyrmions behave as solitonic excitations. We demonstrate the ability to nucleate zero-field skyrmions and move them using electric current pulses, with an efficiency similar to the best established results of the literature using field-stabilized skyrmions. Beyond an obvious applied interest for applications, this demonstration opens an alternative method to stabilize skyrmions, as compared to the litterature. This may be used in antiferromagnetic situations, where a magnetic field cannot be applied to the samples.

ACKNOWLEDGMENTS

We acknowledge fruitful discussions with André Thiaville. This work was supported as a collaborative project by the Indo-French Centre for the Promotion of Advanced Research (IFCPAR/CEFIPRA) (IFC/5808-1/2017), by the French National Research Agency (ANR), under Contract No. ANR-17-CE24-0025 (TopSky), and a public grant overseen by the ANR as part of the "Investissements d'Avenir" program (Labex NanoSaclay, reference: ANR-10-LABX-0035, SPICY).

[1] A. Fert, V. Cros, and J. Sampaio, Skyrmions on the track, Nat. Nanotechnol. **8**, 152 (2013).

[2] X. Zhang, G. P. Zhao, H. Fangohr, J. P. Liu, W. X. Xia, J. Xia, and F. J. Morvan, Skyrmion-skyrmion and skyrmion-edge repulsions in skyrmion-based racetrack memory, Sci. Rep. **5**, 7643 (2015).

[3] K. M. Song, J.-S. Jeong, B. Pan, X. Zhang, J. Xia, S. Cha, T.-E. Park, K. Kim, S. Finizio, and J. Raabe, *et al.*, Skyrmion-based artificial synapses for neuromorphic computing, Nat. Elec. **3**, 148 (2020).

[4] J. Sampaio, V. Cros, S. Rohart, A. Thiaville, and A. Fert, Nucleation, stability and current-induced motion of isolated magnetic skyrmions in nanostructures, Nat. Nanotechnol. **8**, 839 (2013).

[5] S. Woo, K. Litzius, B. Krüger, M.-Y. Im, L. Caretta, K. Richter, M. Mann, A. Krone, R. M. Reeve, and M. Weigand, *et al.*, Observation of room-temperature magnetic skyrmions and their current-driven dynamics in ultrathin metallic ferromagnets, Nat. Mater. **15**, 501 (2016).

[6] F. Büttner, I. Lemesh, and G. S. D. Beach, Theory of isolated magnetic skyrmions: From fundamentals to room temperature applications, Sci. Rep. **8**, 4464 (2015).

[7] N. Romming, A. Kubetzka, C. Hanneken, K. von Bergmann, and R. Wiesendanger, Field-Dependent Size and Shape of Single Magnetic Skyrmions, Phys. Rev. Lett. **114**, 177203 (2015).

[8] C. Moreau-Luchaire, C. Moutafis, N. Reyren, J. Sampaio, C. A. F. Vaz, N. Van Horne, K. Bouzehouane, K. Garcia, C. Deranlot, and P. Warnicke, *et al.*, Additive interfacial chiral interaction in multilayers for stabilization of small individual skyrmions at room temperature, Nat. Nanotechnol. **11**, 444 (2016).

[9] O. Boulle, J. Vogel, H. Yang, S. Pizzini, D. de Souza Chaves, A. Locatelli, T. O. Mentes, A. Sala, L. D. Buda-Prejbeanu, and O. Klein, *et al.*, Room-temperature chiral magnetic skyrmions in ultrathin magnetic nanostructures, Nat. Nanotechnol. **11**, 449 (2016).

[10] W. Jiang, P. Upadhyaya, W. Zhang, G. Yu, M. B. Jungfleisch, F. Y. Fradin, J. E. Pearson, Y. Tserkovnyak, K. L. Wang, and O. Heinonen, *et al.*, Blowing magnetic skyrmion bubbles, Science **349**, 283 (2015).

[11] X. Z. Yu, N. Kanazawa, Y. Onose, K. Kimoto, W. Z. Zhang, S. Ishiwata, Y. Matsui, and Y. Tokura, Real-space observation of a two-dimensional skyrmion crystal, Nature **465**, 901 (2010).

[12] A. Hrabec, J. Sampaio, M. Belmeguenai, I. Gross, R. Weil, S. M. Chérif, A. Stashkevich, V. Jacques, A. Thiaville, and S. Rohart, Current-induced skyrmion generation and dynamics in symmetric bilayers, Nat. Commun. **8**, 15765 (2017).

[13] S. Rohart and A. Thiaville, Skyrmion confinement in ultrathin film nanostructures in the presence of Dzyaloshinskii-Moriya interaction, Phys. Rev. B **88**, 184422 (2013).

[14] C. Back, V. Cros, H. Ebert, K. Everschor-Sitte, A. Fert, M. Garst, T. Ma, S. Mankovsky, T. L. Monchesky, and M. Mostovoy, *et al.*, The 2020 skyrmionics roadmap, J. Phys. D: Appl. Phys. **53**, 363001 (2020).

[15] J. Barker and O. A. Tretiakov, Static and Dynamical Properties of Antiferromagnetic Skyrmions in the Presence of Applied Current and Temperature, Phys. Rev. Lett. **116**, 147203 (2016).

[16] Y. Hirata, D.-H. Kim, S. K. Kim, D.-K. Lee, S.-H. Oh, D.-Y. Kim, T. Nishimura, T. Okuno, Y. Futakawa, and H. Yoshikawa, *et al.*, Vanishing skyrmion Hall effect at the angular momentum compensation temperature of a ferrimagnet, Nat. Nanotechnol. **14**, 232 (2019).

[17] L. Caretta, M. Mann, F. Büttner, K. Ueda, B. Pfau, C. M. Günther, P. Hessing, A. Churikova, C. Klose, and M. Schneider, *et al.*, Fast current-driven domain walls and small skyrmions in a compensated ferrimagnet, Nat. Nanotechnol. **13**, 1154 (2018).

[18] X. Zhang, Y. Zhou, and M. Ezawa, Magnetic bilayer-skyrmions without skyrmion Hall effect, Nat. Commun. **7**, 10293 (2016).

[19] W. Legrand, D. Maccariello, F. Ajejas, S. Collin, A. Vecchiola, K. Bouzehouane, N. Reyren, V. Cros, and A. Fert, Room-temperature stabilization of antiferromagnetic skyrmions in synthetic antiferromagnets, Nat. Mater. **19**, 34 (2020).

[20] K. G. Rana, A. Finco, F. Fabre, S. Chouaieb, A. Haykal, L. D. Buda-Prejbeanu, O. Fruchart, S. Le Denmat, P. David, and M. Belmeguenai, *et al.*, Room-Temperature Skyrmions at Zero Field in Exchange-Biased Ultrathin Films, Phys. Rev. Appl. **13**, 044079 (2020).

[21] Y. Guang, I. Bykova, Y. Liu, G. Yu, E. Goering, M. Weigand, J. Gräfe, S. K. Kim, J. Zhang, and H. Zhang, *et al.*, Creating zero-field skyrmions in exchange-biased multilayers through x-ray illumination, Nat. Commun. **11**, 949 (2020).

[22] J. C. Gallagher, K. Y. Meng, J. T. Brangham, H. L. Wang, B. D. Esser, D. W. McComb, and F. Y. Yang, Robust Zero-Field Skyrmion Formation in FeGe Epitaxial Thin Films, Phys. Rev. Lett. **118**, 027201 (2017).

[23] P. Ho, A. K. C. Tan, S. Goolaup, A. L. Oyarce, M. Raju, L. S. Huang, A. Soumyanarayanan, and C. Panagopoulos, Geometrically Tailored Skyrmions at Zero Magnetic Field in Multilayered Nanostructures, Phys. Rev. Appl. **11**, 024064 (2019).

[24] N. K. Duong, M. Raju, A. P. Petrovic, R. Tomasello, G. Finocchio, and C. Panagopoulos, Stabilizing zero-field skyrmions in Ir/Fe/Co/Pt thin film multilayers by magnetic history control, Appl. Phys. Lett. **114**, 072401 (2019).

[25] M. Li, A. Rai, A. Pokhrel, A. Sapkota, C. Mewes, T. Mewes, M. D. Graef, and V. Sokalski, Formation of zero-field skyrmion arrays in asymmetric superlattices, Appl. Phys. Lett. **117**, 112403 (2020).

[26] J. B. ao, D. Dugato, M. Puydinger dos Santos, F. Béron, and J. Cezar, Tuning isolated zero-field skyrmions and spin spirals at room-temperature in synthetic ferrimagnetic multilayers, Appl. Surf. Sci. **585**, 152598 (2022).

[27] D. Bhattacharya, S. A. Razavi, H. Wu, B. Dai, K. L. Wang, and J. Atulasimha, Creation and annihilation of non-volatile fixed magnetic skyrmions using voltage control of magnetic anisotropy, Nat. Elec. **3**, 539 (2020).

[28] I. Lemesh, K. Litzius, M. Böttcher, P. Bassirian, N. Kerber, D. Heinze, J. Zázvorka, F. Büttner, L. Caretta, and M. Mann, *et al.*, Current-Induced Skyrmion Generation through Morphological Thermal Transitions in Chiral Ferromagnetic Heterostructures, Adv. Mater. **30**, 1805461 (2018).

[29] S. Meyer, M. Perini, S. von Malottki, A. Kubetzka, R. Wiesendanger, K. von Bergmann, and S. Heinze, Isolated zero field sub-10 nm skyrmions in ultrathin Co films, Nat. Commun. **10**, 3823 (2019).

[30] K. Fallon, S. Hughes, K. Zeissler, W. Legrand, F. Ajejas, D. Maccariello, S. McFadzean, W. Smith, D. McGrouther, and S. Collin, *et al.*, Controlled individual Skyrmion nucleation at artificial defects formed by ion irradiation, Small **16**, 1907450 (2020).

[31] K. Litzius, I. Lemesh, B. Krüger, P. Bassirian, L. Caretta, K. Richter, F. Büttner, K. Sato, O. A. Tretiakov, J. Förster, and *et al.*, Skyrmion Hall effect revealed by direct time-resolved x-ray microscopy, Nat. Phys. **13**, 170 (2017).

[32] W. Jiang, X. Zhang, G. Yu, W. Zhang, X. Wang, M. BenjaminJungfleisch, J. Pearson, X. Cheng, O. Heinonen, and K. L. Wang, *et al.*, Direct observation of the skyrmion Hall effect, Nat. Phys. **13**, 162 (2017).

[33] A. Hrabec, V. Křižáková, S. Pizzini, J. a. Sampaio, A. Thiaville, S. Rohart, and J. Vogel, Velocity Enhancement by Synchronization of Magnetic Domain Walls, Phys. Rev. Lett. **120**, 227204 (2018).

[34] See the Supplemental Material at http://link.aps.org/supplemental/10.1103/PhysRevApplied.18.064072 for experimental details about the sample growth, magnetic characterization, and additionnal data about zero-field current-induced skyrmion nucleation.

[35] H. Yang, A. Thiaville, S. Rohart, A. Fert, and M. Chshiev, Anatomy of Dzyaloshinskii-Moriya Interaction at Co/Pt Interfaces, Phys. Rev. Lett. **115**, 267210 (2015).

[36] P. Géhanne, S. Rohart, A. Thiaville, and V. Jeudy, Strength and length scale of the interaction between domain walls and pinning disorder in thin ferromagnetic films, Phys. Rev. Res. **2**, 043134 (2020).

[37] V. Grolier, D. Renard, B. Bartenlian, P. Beauvillain, C. Chappert, C. Dupas, J. Ferré, M. Galtier, E. Kolb, and M. Mulloy, *et al.*, Unambiguous Evidence of Oscillatory Magnetic Coupling between Co Layers in Ultrahigh Vacuum Grown Co/Au(111)/Co Trilayers, Phys. Rev. Lett. **71**, 3023 (1993).

[38] A. Bellec, S. Rohart, M. Labrune, J. Miltat, and A. Thiaville, Domain wall structure in magnetic bilayers with perpendicular anisotropy, EPL (Europhys. Lett.) **91**, 17009 (2010).

[39] J. M. Winter, Bloch wall excitation: Application to nuclear resonance in a Bloch wall, Phys. Rev. **124**, 452 (1961).

[40] I. Gross, W. Akhtar, A. Hrabec, J. Sampaio, L. J. Martínez, S. Chouaieb, B. J. Shields, P. Maletinsky, A. Thiaville, and S. Rohart, *et al.*, Skyrmion morphology in ultrathin magnetic films, Phys. Rev. Mater. **2**, 024406 (2018).

[41] J.-Y. Chauleau, R. Weil, A. Thiaville, and J. Miltat, Magnetic domain walls displacement: Automotion versus spin-transfer torque, Phys. Rev. B **82**, 214414 (2010).

[42] J. Torrejon, G. Malinowski, M. Pelloux, R. Weil, A. Thiaville, J. Curiale, D. Lacour, F. Montaigne, and M. Hehn, Unidirectional Thermal Effects in Current-Induced Domain Wall Motion, Phys. Rev. Lett. **109**, 106601 (2012).

[43] C. Kooy and U. Enz, Experimental and theoretical study of the domain configuration in thin layers of $BaFe_{12}O_{19}$, Philips Res. Rep. **15**, 7 (1960).

[44] A. Bernand-Mantel, C. B. Muratov, and T. M. Simon, Unraveling the role of dipolar versus Dzyaloshinskii-Moriya interactions in stabilizing compact magnetic skyrmions, Phys. Rev. B **101**, 045416 (2020).

[45] A. Thiele, Application of the gyrocoupling vector and dissipation dyadic in the dynamics of magnetic domains, J. Appl. Phys. **45**, 377 (1974).

[46] O. Heinonen, W. Jiang, H. Somaily, S. G. E. te Velthuis, and A. Hoffmann, Generation of magnetic skyrmion bubbles by inhomogeneous spin Hall currents, Phys. Rev. B **93**, 094407 (2016).

[47] J. Gorchon, J. Curiale, A. Lemaître, N. Moisan, M. Cubukcu, G. Malinowski, C. Ulysse, G. Faini, H. J. von Bardeleben, and V. Jeudy, Stochastic Current-Induced Magnetization Switching in a Single Semiconducting Ferromagnetic Layer, Phys. Rev. Lett. **112**, 026601 (2014).

[48] K. Litzius, J. Leliaert, P. Bassirian, D. Rodrigues, S. Kromin, I. Lemesh, J. Zazvorka, K.-J. Lee, J. Mulkers, and N. Kerber, *et al.*, The role of temperature and drive current in skyrmion dynamics, Nat. Electron. **3**, 30 (2020).

[49] Y. Tokura and N. Kanazawa, Magnetic skyrmion materials, Chem. Rev. **121**, 2857 (2021).

[50] S. Pizzini, J. Vogel, S. Rohart, L. D. Buda-Prejbeanu, E. Jué, O. Boulle, I. M. Miron, C. K. Safeer, S. Auffret, and G. Gaudin, *et al.*, Chirality-Induced Asymmetric Magnetic Nucleation in Pt/Co/AlO_x Ultrathin Microstructures, Phys. Rev. Lett. **113**, 047203 (2014).

[51] M. Belmeguenai, J.-P. Adam, Y. Roussigné, S. Eimer, T. Devolder, J.-V. Kim, S. M. Cherif, A. Stashkevich, and A. Thiaville, Interfacial Dzyaloshinskii-Moriya interaction in perpendicularly magnetized Pt/Co/AlO_x ultrathin films measured by Brillouin light spectroscopy, Phys. Rev. B **91**, 180405(R) (2015).

[52] K.-J. Kim, J.-C. Lee, S.-M. Ahn, K.-S. Lee, C.-W. Lee, Y. J. Cho, S. Seo, K.-H. Shin, S.-B. Choe, and H.-W. Lee, Interdimensional universality of dynamic interfaces, Nature **458**, 740 (2009).

[53] V. Jeudy, A. Mougin, S. Bustingorry, W. Savero Torres, J. Gorchon, A. B. Kolton, A. Lemaître, and J.-P. Jamet, Universal Pinning Energy Barrier for Driven Domain Walls in Thin Ferromagnetic Films, Phys. Rev. Lett. **117**, 057201 (2016).